Electro-Chemo-Mechanical Failure of Solid Electrolytes Induced by Growth of Internal Lithium Filaments

ADVANCED MATERIALS
www.advmat.de

Electro–Chemo–Mechanical Failure of Solid Electrolytes Induced by Growth of Internal Lithium Filaments

Xieyu Xu, Yangyang Liu, Olesya O. Kapitanova, Zhongxiao Song, Jun Sun, and Shizhao Xiong**

Growth of lithium (Li) filaments within solid electrolytes, leading to mechanical degradation of the electrolyte and even short circuit of the cell under high current density, is a great barrier to commercialization of solid-state Li-metal batteries. Understanding of this electro–chemo–mechanical phenomenon is hindered by the challenge of tracking local fields inside the solid electrolyte. Here, a multiphysics simulation aiming to investigate evolution of the mechanical failure of the solid electrolyte induced by the internal growth of Li is reported. Visualization of local stress, damage, and crack propagation within the solid electrolyte enables examination of factors dominating the degradation process, including the geometry, number, and size of Li filaments and voids in the electrolyte. Relative damage induced by locally high stress is found to preferentially occur in the region of the electrolyte/Li interface having great fluctuations. A high number density of Li filaments or voids triggers integration of damage and crack networks by enhanced propagation. This model is built on coupling of mechanical and electrochemical processes for internal plating of Li, revealing evolution of multiphysical fields that can barely be captured by the state-of-the-art experimental techniques. Understanding mechanical degradation of solid electrolytes with the presence of Li filaments paves the way to design advanced solid electrolytes for future solid-state Li-metal batteries.

1. Introduction

To realize a carbon neutral society, there is a strong driving force to develop advanced battery technologies with high energy density and high safety for mobile applications such as electric vehicles, consumer electronics, and smart grid.[1] The pathway for gaining these targets is to build new battery chemistry by exploration of high-capacity anode and cathode materials as well as nonflammable electrolytes.[2,3] Metallic anodes, represented by lithium (Li), were the promising anode materials owing to their high theoretical capacity and it is, for instance, as high as 3860 mAh g^{-1} for Li-metal anodes.[4,5] Nevertheless, the non-uniform electrodeposition of Li metal during the charging process invariably leads to low Coulombic efficiency and growth of Li dendrites, hindering its commercialization in rechargeable batteries.[6–8]

Utilization of solid electrolytes with high shear modulus was known as the most promising approach to suppress the formation of Li dendrites and to guarantee high safety of the battery at the same time.[9] Despite the significant advances aiming for high ionic conductivity of solid electrolytes, operation of solid-state batteries under the practical industry conditions, particularly for high-power systems, is not achieved yet.[10] A cell failure induced by the propagation of Li filaments (or Li dendrites) through solid electrolytes will be triggered once the applied current density is over a certain value which is defined as critical current density.[11] The growth of Li filaments leads to the failure of physical contact at interface, mechanical degradation of solid electrolyte, and even the short circuit of cell when the filaments connect the anode with cathode.[12] These failure processes have been reported for various solid electrolytes, including garnet $Li_7La_3Zr_2O_{12}$(LLZO),[13] amorphous $70Li_2S$-$30P_2S_5$ glass,[14] argyrodite (Li_6PS_5Cl),[15] and sodium superionic conductor type (NASICON, such as $Li_{1+x}Al_xGe_{2-x}(PO_4)_3$).[16]

Capturing the formation and the propagation of Li filaments in solid electrolyte to understand the failure mechanism of solid-state batteries is a great challenge since the microstructure evolution of interest is buried inside the solid electrolyte.[10] State of the art characterization techniques including operando synchrotron X-ray tomographic microscopy,[17] in situ transmission electron microscopy,[18] and operando neutron depth profiling[13] have been employed to track the internal evolution of solid electrolyte in real time by the combination of electrochemical methodologies. It is found that origin of Li filaments

X. Xu, Y. Liu, O. O. Kapitanova, Z. Song, J. Sun
State Key Laboratory for Mechanical Behavior of Materials
Xi'an Jiaotong University
Xi'an 710049, P. R. China
E-mail: liuyy123@stu.xjtu.edu.cn
S. Xiong
Department of Physics
Chalmers University of Technology
Göteborg SE 412 96, Sweden
E-mail: shizhao.xiong@chalmers.se
The ORCID identification number(s) for the author(s) of this article can be found under https://doi.org/10.1002/adma.202207232.

DOI: 10.1002/adma.202207232

inside solid electrolyte can be attributed to two mechanisms, Li propagation following the interfacial cracks induced by higher local stress field as well as current density,[14,15,17] and Li deposition at grain boundaries of solid electrolyte due to the reduced bandgap or the high electronic conductivity.[13,18] After filling the primary cracks, the ongoing plated Li will generate sufficient stress under the driving overpotential to promote the extension of Griffith-like cracks[14] and the high local strain around new formed cracks has been captured by digital volume correlation analysis of X-ray computed tomograms.[19] The propagation and relaxation of Li filaments inside cracks create various morphology evolution and different geometries of plated Li, for instance, "straight" type, "spalling" type, "branching" type, and "diffuse" type.[20] The geometry of Li filaments and applied current density are critical for determining the propagation rate or the failure time of solid-state cell which is resulted from the internal short circuit.

There is no doubt that the crack extension inside solid electrolyte, which is induced by Li-plating stress, is of great significance for understanding the failure of solid-state cells since this mechanical degradation will increase the internal impedance and provide pathway for internal connection of Li filaments, directly related to the electrochemical performance of the battery.[16,19] However, precise measurement of local stress and current density inside solid electrolyte has not been possible although the phenomena of failure processes can be observed by advanced techniques. Therefore, electro–chemo–mechanical models have been built to explain the infiltration of Li filaments from the perspective of physical fields.[14,21] In these models the geometries of Li filaments are usually simplified as pre-defects with a standard configuration. Consequently, the fundamental correlations between the key parameters (geometries, size, distribution) of Li filaments and the mechanical degradation of solid electrolyte have not been well understood, restricting the experimental efforts of designing efficient strategies to suppress the propagation of Li filaments in future solid-state batteries.

In this work, we build an electro–chemo–mechanical model for the crack propagation in solid electrolyte (NASICON-type, $Li_{1.3}Al_{0.3}Ge_{1.7}(PO_4)_3$ [LAGP]), which is induced by the stress from electrochemical plating of Li. The local distributions of stress, displacement, relative damage, and corresponding crack propagation are visualized based on the method of multiphysics simulation, which has shown a great potential to fill gap between modeling conditions and real situation in electrochemical systems.[22] Therefore, it allows us to reveal the mechanical evolution of bulk solid electrolyte with the growth of Li filaments inside. The key parameters of Li filaments, including the geometry, number density, and diameter, are evaluated to show their influence on the crack propagation process of solid electrolyte. Moreover, the pre-existing voids, which are commonly obtained in real ceramic solid electrolytes,[23–25] also present a significant impact on the propagation of Li filaments and the resulted cracks. Our work shows a great promise to comprehensively understand the failure mechanism of solid electrolyte induced by the growth of Li filaments, and further provides a general method to simulate the mechanical degradation of solid electrolyte correlated to electrochemical process.

2. Results and Discussion

2.1. Role of Li Filament Geometry on Failure of Solid Electrolyte

The geometry of Li filaments in soliFd electrolyte has been revealed as triangle at the triple junction,[18] cylindrical whiskers or dendrites,[26,27] and sheet-like or branch-like,[19,20,28] by experimental techniques. It is found that the geometry of Li filament is shaped by current density, solid electrolyte, and local fields.[15,20,29] Here, typical geometries for a single Li filament, cylinder, elliptical cylinder, triangular prism, and cube, are chosen to investigate the local effect of the geometry on the failure process of solid electrolyte in bulk. As seen in the distribution of von Mises stress caused by the growth of Li filament, the region surrounding the Li filament shows an obvious stress increase, which is induced by the extrusion from the circumferential expansion of Li filament (**Figure 1** and Figure S1, Supporting Information). Along with the growth of Li filament, the area with higher stress gradually enlarges. Typically, when the geometry of Li filament is set as the cylinder, the high-stress region is relatively uniform compared with that created by Li filaments with other geometries (Figure 1a). Moreover, the high-stress region will be separated when there is structural fluctuation on edge of the Li filaments. Two separated regions show up in parallel with the ellipse axis when the geometry of Li filament changes to the elliptical cylinder (Figure 1b). Three and four separated regions are seen in parallel with the sides of triangle and rectangle when the geometry of Li filament inside solid electrolyte appears as triangle prism and cube, respectively (Figure 1c,d). It is worth noting that the boundaries that separate the different high-stress regions exhibit relative low stress, which can be considered as the release of stress and the initiation of local displacement.

The stress distribution along the *X*-axis and *Y*-axis was further derived from the marked regions in Figure 1a–d. As shown in Figure 1e,f, for the geometries with same structure along th *X*- and *Y*-axis, the extrema of von Mises stress around the Li filament with the geometry of cylinder and cube are quite close, while a faster rate is observed for stress formation around cylindrical Li filament (Figure S2, Supporting Information). For the geometries of elliptical cylinder and triangular prism, the distributions of von Mises stress are heterogeneous along the direction of the *X*-axis and the *Y*-axis. For the directions of the *X*-axis and the *Y*-axis, the extrema around the elliptical Li filament are higher than that around the triangular prism. In addition, the rate of stress formation around elliptical Li filament is higher than that for triangular-prism Li filament. For the whole distribution of stress (Figure S3, Supporting Information), high local stress surrounding the Li filaments with geometries of cube and elliptical cylinder is more possible to induce the locally circumferential deformation of solid electrolyte and to trigger the damage in the corresponding region. It is worth noting that the great structural fluctuation at the corner of cube or the vertex of elliptical cylinder is responsible to the stress concentration.

As the consequence of the distribution of von Mises stress, the resulted deformation of solid electrolyte happens around the Li filaments and the statistics of its distribution was shown in the plots with violin profile (**Figure 2**a). The deformation within

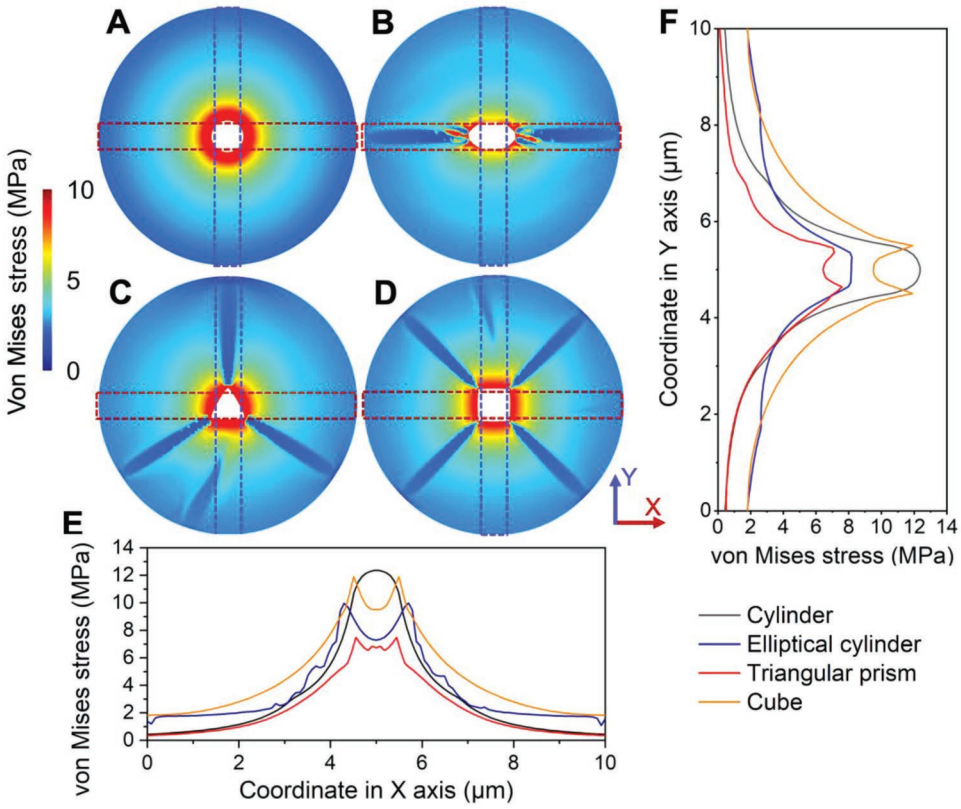

Figure 1. Distribution of stress around Li filaments with various geometries inside solid electrolyte. a–d) Visualization of the von Mises stress around the Li filaments with the geometries of cylinder (a), elliptical cylinder (b), triangular prism (c), and cube (d). e,f) Distribution of von Mises stress along the *X*-axis (e) and *Y*-axis (f) after equal calculation times.

solid electrolytes containing Li filaments of various geometries shows distinctive distribution along the *X*- and *Y*-axis. When Li filament is a circumferentially isotropic cylinder, the deformation in all directions, especially on the *X*- and *Y*-axes, is the same. The deformation changes to an anisotropic distribution in the circumferential direction with the structural fluctuation arising on the sides of Li filament with geometries of elliptical cylinder, triangular, or cube. Taking the elliptical cylinder as an example, the deformation of solid electrolyte along the *Y*-axis is greater than that in parallel with the *X*-axis, which means that two regions separated by the ellipse have moved in the opposite directions. Transferring this insight to the Li filaments of triangular prism and cube, it is found that any region facing the side of the triangular or square shows deformation vertical to the corresponding side. Furthermore, the sums of crack and related damage were calculated to investigate the failure process of solid electrolytes caused by the growth of various Li filaments. As shown in Figure 2b, within the same calculating time of 3.5 s, the cylindrical Li filament endows solid electrolyte with the smallest crack even with the sum damage of 761 and the sum crack of 153. In contrast, damages caused by the growth of Li filament with the geometries of elliptical cylinder, triangular prism, and cube are 886, 171, and 934, forming cracks of 586, 102, and 399, respectively. Among them, the exception about triangular prism can be interpreted that the damage speed is relatively lower than others. To be more precise, the linear coefficient between damage and crack is proposed to illustrate that the failure of solid electrolyte caused by cylindrical Li filament is least among the other geometries.

Furthermore, the growth of Li filament with the geometry of cylinder, elliptical cylinder, triangular prism, and cube takes a calculating time of 6, 3.67, 7.8, and 3.92 s, respectively, till the solid electrolyte is completely broken (Figure S4, Supporting Information). The calculating time at convergence state shows a strong dependence on the geometry of internal Li filaments. As shown in Figure 2c, a sum damage of 3160 is mainly distributed around the cylinder. When the geometries of Li filament change to elliptical cylinder, triangular prism, and cube, the damage region mainly distributes along the extended line of each corner and exhibits radial shape as a whole (Figure 2d–f and Figure S5, Supporting Information). Moreover, the degree of damage represented by the sum damage is greater with the increase of isotropy of Li filament (1826 for elliptical cylinder, 2036 for triangular prism, and 2653 for cube). Once the damage exceeds by the fracture limit of solid electrolyte, the crack shows up reasonably. As shown in Figure 2g, the smallest crack arises around the cylindrical Li filament, and the cracks place on the extended line of the corners of the Li filaments with geometries of elliptical cylinder, triangular prism, and cube (Figure S6, Supporting Information). Surprisingly, both the maximum crack (the highest value of crack on a particular solid electrolyte pellet) and the maximum sum crack (the highest value of sum crack calculated by summating all cracks on one solid electrolyte pellet) are found in solid electrolyte with

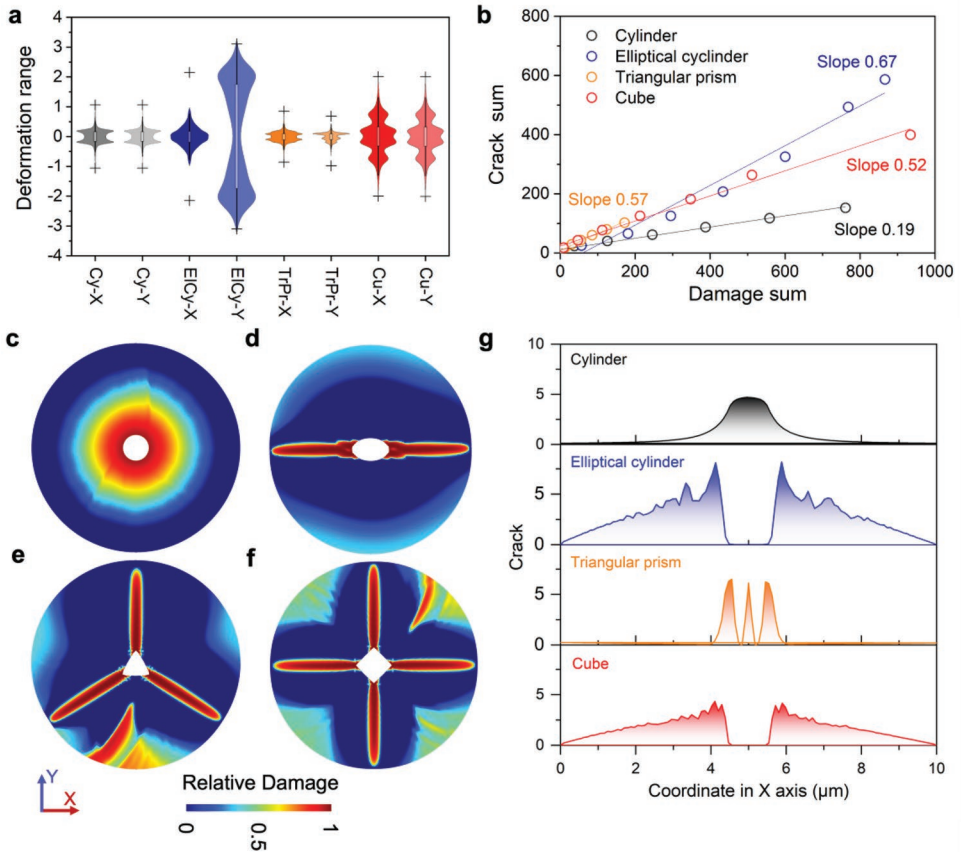

Figure 2. Bulk failure of solid electrolyte with Li filaments inside. a) Deformation of solid electrolyte after Li filament's expansion with geometries of cylinder (Cy-*X*, Cy-*Y*), elliptical cylinder (ElCy-*X*, ElCy-*Y*), triangular prism (TrPr-*X*, TrPr-*Y*), and cube (Cu-*X*, Cu-*Y*) along the *X*- and *Y*-axes, respectively. b) Relationship between crack and damage inside the solid electrolyte during growth of the Li filament after a certain calculating time of 3.5 s. c–f) Relative damage of solid electrolyte around Li filaments with geometries of cylinder (c), elliptical cylinder (d), triangular prism (e), and cube (f) at the convergence state of the calculation. g) Crack distribution of the solid electrolyte around the Li filaments along the *X*-axis.

Li filament of elliptical cylinder inside (Figure 2g and Figure S7, Supporting Information). It is worth noting that the propagation of cracks is not a process with constant speed and thus the failure time cannot be directly correlated to the sum crack. The investigation of the stress and corresponding damage evolution as well as the crack distribution indicates that the growth of Li filament inside solid electrolyte inevitably leads to the damage of solid electrolyte and generates the crack, which has been widely accepted as one reason for the failure of solid-state batteries.[13,18] Our results suggest that the geometry of Li filaments plays a critical role on the disintegrating process of solid electrolyte induced by the circumferential stress.

2.2. Failure of Solid Electrolyte with Multiple Li Filaments Inside

Previous experimental results show that the configuration of Li filaments in real solid electrolyte is usually formed with network structure that contains multiple branches.[19,20] Therefore, the failure process of a real solid electrolyte will be more complicated and the interplay between contiguous Li filaments will influence the local fields. To make our modeling closer to reality, the investigation of the failure of solids electrolyte was expanded to a complex model containing multiple Li filaments, of which the geometry is selected as cylinder. The size and number of multiple Li filaments are varied whereas the total volume of Li filaments in one series with different sizes (such as S-9, M-3, and L-1) is fixed. The relative position of Li filaments inside solid electrolyte was generated using random function, see details in the Experimental Section. Combining with the visualization of stress distribution (Figure S8, Supporting Information), it is found that von Mises stress in solid electrolyte shows two classes of distribution, around the isolated Li filaments and linkage between two adjacent Li filaments. When the number of Li filament is small, there is only lighter stress surrounding the filaments. With the increasing number of filaments, stress field propagates and integrates as a connected region of higher stress within the solid electrolyte. For small-size Li filaments (Figure S8a–d, Supporting Information), the mean distance between two filaments is shortened with the increase of its number, resulting in an integrated stress field covering the adjacent filaments. Moreover, the adjacent filaments are linked by the low stress region probably caused by the release of stress from local displacement. In contrast, the integrated stress field between adjacent filaments is weakened with the enlargement of Li filaments size (Figure S8e–l, Supporting Information).

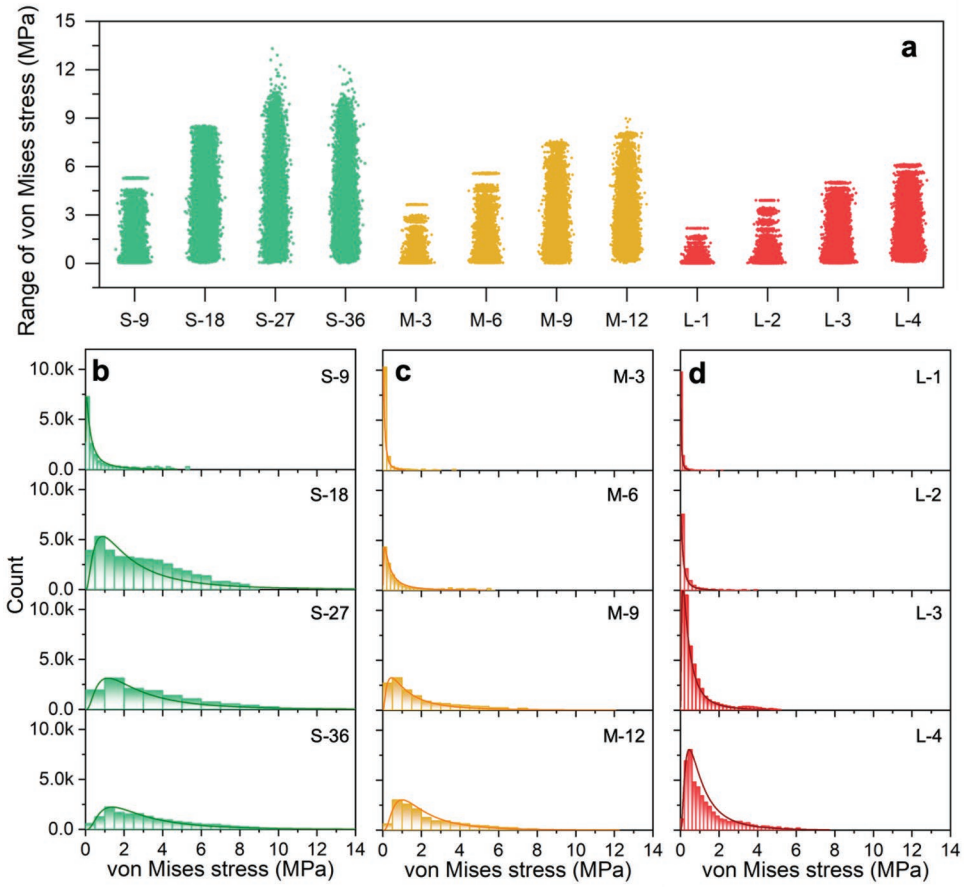

Figure 3. Distribution of von Mises stress inside solid electrolyte with multiple Li filaments. a) Range of von Mises stress inside solid electrolyte induced by growth of multiple Li filaments. Total volume of Li filaments with various sizes was set as equal and the geometry of Li filaments is fixed as cylinder. S-9, 18, 27, and 36 represent Li filaments in small size and with number of 9, 18, 27, and 36 in the same model volume. M-3, 6, 9, and 12 represent Li filaments in medium size and with number of 3, 6, 9, and 12. L-1, 2, 3, and 4 represent Li filaments in large size and with number of 1, 2, 3, and 4. b–d) Frequency histograms for distribution of von Mises stress inside solid electrolyte with multiple Li filaments in small (b), medium (c), and large (d) size.

The von Mises stress is further counted to precisely uncover the relationship between its distribution and the Li filament size as well as number, indicating the corresponding failure process of solid electrolyte. The von Mises stress decreases with the increase of Li filament size while it increases with the rising number of filaments inside solid electrolyte (**Figure 3**a). The frequency histogram (Figure 3b–d) for von Mises stress within solid electrolyte containing multiple Li filaments shows a lognormal distribution. Moreover, the distribution of von Mises stress in solid electrolyte shifts to being wider with the increasing number of small Li filaments. For example, the distribution of high stress with 36 small-size Li filaments is greater compared with that only containing 9 (Figure 3b). The same tendency shows up with the medium- and large-size Li filaments (Figure 3c–d). Therefore, under the condition of same volume of Li inside solid electrolyte, less-and-large Li filaments contribute to lower stress, while plenty-and-small Li filaments endow the bulk of solid electrolyte with locally high stress field.

Under the assumption that solid electrolyte is a continuum, the generated stress field from the growth of Li filaments will invariably result in the local displacement inside solid-state electrolyte. The displacement maps in **Figure 4**a–l reveal that the bulk of solid electrolytes show two displacement behaviors. The region out of the connection area between Li filaments is pushed away from the main body of solid electrolytes. By contrast, the region surrounded by the filaments does not appear to be remarkably displaced despite being squeezed inwardly. These displacement behaviors are consistent with previous strain maps from digital volume correlation analysis on the X-ray tomographic scans of solid electrolyte pellets.[15,16,19] The maps for small-size Li filaments are taken as an example to discuss in detail (Figure 4a–d). The final displacement, which is the superposition of multiple position shifts, is governed by the synergy from the number of Li filaments and related positions inside the solid electrolytes. The number of the local regions with different-level displacement is increasing with the increased amount of Li filaments inside. As shown in Figure 4m and Table S1, Supporting Information, the maximum displacement of the solid electrolyte increases with the higher number of Li filaments, indicating the greater damage effect caused by the growth of Li filaments.

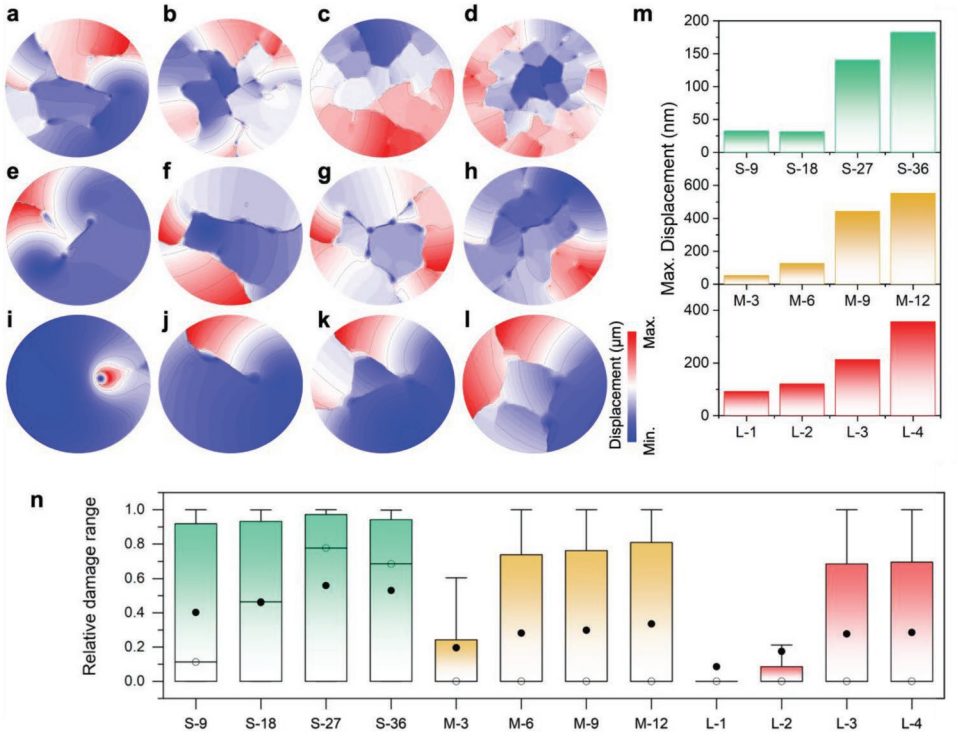

Figure 4. Mechanical failure of solid electrolyte caused by growth of multiple Li filaments. a–l) Displacement of solid electrolyte caused by growth of 9 (a), 18 (b), 27 (c), and 36 (d) small-size Li filaments (S-9, 18, 27, and 36); 3 (e), 6 (f), 9 (g), and 12 (h) medium-sized Li filaments (M-3, 6, 9, and 12); and 1 (i), 2 (j), 3 (k), and 4 (l) large-size Li filaments (L-1, 2, 3, and 4). m) Maximum displacement of solid electrolyte with different Li filaments. Total volume of Li filaments with different size inside solid electrolyte was set as equal. n) Distribution of relative damage of solid electrolyte caused by Li filaments with different sizes. Open circles represent the median and filled circles represent the average.

The damaging process of solid electrolyte with small-size Li filaments (Figure S9, Supporting Information) shows that the damage initially occurs at the surrounding region of Li filaments and gradually propagates to the damaged region around the nearest Li filament, followed by the integration of two regions. Eventually, multiple regions of damage within solid electrolyte connect with each other to form a network and time to form the damage network is shortened with the increased amount of Li filaments. The similar damage behavior is obtained for the medium- and large-size multiple Li filaments in solid electrolyte (Figures S10 and S11, Supporting Information), but the degree of damage is lightened with the increase of Li filaments' size. Here, it is worth noticing that with the same total volume of Li the number of damage degree is less for large-size filaments. Eventually, the damage caused by the growth of multiple filaments is catastrophic to the integrity of solid electrolytes when the network of the damage regions is formed (Figure S12, Supporting Information). Moreover, the derived damage values were shown in the box plot and the relative damage of 1, that means completely damage, is observed for almost all cases except the solid electrolytes with one and two large-size Li filaments and three medium-size Li filaments (Figure 4n). The averaged damage caused by the Li filaments with small size is greater than that with the larger size. With the small-size Li filaments, the damage degree is obviously enhanced with the increased amount of Li filaments from 9 to 36, illustrated by the average and median in boxes. Frequency histogram for damage distribution (Figure S13, Supporting Information) indicates that the count of high damage in solid electrolytes increases with the raised number of filaments. Eventually, the generation of cracks shows that growth of Li filaments will lead to the disintegration of solid electrolyte, and the broken degree is dependent on the amount of Li filaments (Figures S14 and S15, Supporting Information). The failure time for solid electrolytes (Figure S16, Supporting Information) also reveals that the time is shortened with the increased number of Li filaments and their small size.

2.3. Failure of Solid Electrolyte Caused by Li Filaments with Presence of Voids

In a real solid electrolyte pellet, a certain number of internal voids is inevitably formed during the sintering process due to the distribution of grain size, relative density change, anisotropic growth of grains, etc.[23,30,31] In this study, the pre-existing voids in solid electrolyte were taken into account to visualize the damage process and to evaluate the effect of size and number of voids on the failure of solid electrolyte with certain amount of Li filaments inside. As shown in **Figure 5**a, the high-stress regions caused by the compression from the growth of Li filaments mainly surround the Li filaments, and they can be disturbed by the near stress field to show radial shape. The interior of two high-stress regions between Li filaments presents an under-stress region, illustrating the stress-releasing for the local displacement. Moreover, the high-stress regions tend to

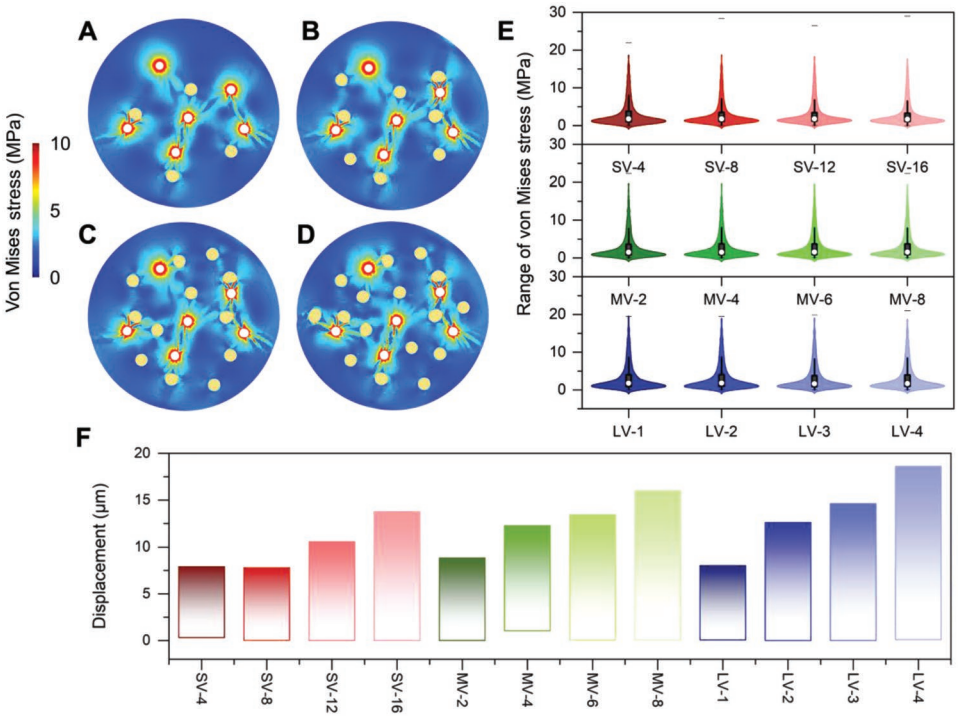

Figure 5. Effect of voids inside solid electrolyte on von Mises stress field. a–d) Distribution of von Mises stress inside the solid electrolyte with 4 (a), 8 (b), 12 (c), and 16 (d) small-size voids and 6 grown Li filaments. Voids and Li filaments are represented by brown regions and white regions, respectively. The calculation time is 2.5 s. e) Distribution of von Mises stress within solid electrolyte containing different size voids and multiple grown Li-filaments. Total volume of voids with different size was set as equal and the geometry of voids is fixed as cylinder. SV-4, 8, 12, and 16 represent voids in small size and with number of 4, 8, 12, and 16 in the same modeling volume. MV-2, 4, 6, and 8 represent voids in medium size and with number of 2, 4, 6, and 8. LV-1, 2, 3, and 4 represent voids in large size and with number of 1, 2, 3, and 4. f) Minimum and maximum displacement of solid electrolyte with various voids and multiple grown Li filaments.

connect with each other, and their propagation can bypass the internal voids. Within the same damaging time of 2.5 s, the distribution of von Mises stress shows a negligible difference with the increased number of voids inside, varying from 4 to 16 (Figure 5a–d). The same tendency for the distribution of von Mises stress can be observed inside the bulk of electrolytes with medium- and large-size voids (Figure S17, Supporting Information, and Figure 5e).

Also, the statistics of damage value shows the similar distributions, including the logarithm distribution, median, maximum as well as the minimum (Figure S18, Supporting Information). However, the failure time of solid electrolytes with different internal voids varies, which prolongs with the increased number of voids and is slightly affected by the size of voids (Figure S19, Supporting Information). After the convergence of calculation, the distinguished reinforcement is shown up in the high-stress regions between Li filaments and their propagation phenomenon around voids is more pronounced (Figure S20, Supporting Information). The discreteness for the distribution of von Mises stress is enlarged with the increased number of voids. The displacement of solid electrolyte caused by the stress field with presence of voids shows that the regions out of the continuous stress network move outward and the moving degree is strengthened with the increased number of voids with small, medium, and large sizes (Figure 5f and Figure S21, Supporting Information). Therefore, the number of internal voids delivers a more significant effect on the stress and displacement fields as compared to the size.

The result of the displacement is the damage around the Li filaments, which exceeds the fracture time of solid electrolyte to create the crack inside. The distributions of damage coupled with crack in the solid electrolyte with voids and Li filaments are shown in **Figure 6**. The damage regions surround each filament and propagate between Li filaments. It is worth noting that the damage region can pass through the internal voids due to the spread of stress surrounding the voids and the resulted deformation of voids. From the relationship between stress distribution and the existence of internal voids, it is found that the damage level and local distribution are affected by the number of internal voids and their relative position toward Li filaments. When the internal voids are in small size (Figure 6a–d), the damage region enlarges with the increased number of internal voids. Meanwhile, the corresponding cracks witness widening with lengthening. Similar tendency is obtained for the solid electrolytes with medium and large size internal voids (Figure 6e–l). In terms of the size of voids with equal volume in total, both damage regions and corresponding cracks show little difference with the decrease of void size, as shown in Figure 6a,e,i. The disintegration of solid electrolyte represented with the damage sum and corresponding crack sum (Figure 6m and Figure S22, Supporting Information) is obviously increasing with the higher amount of voids. Therefore,

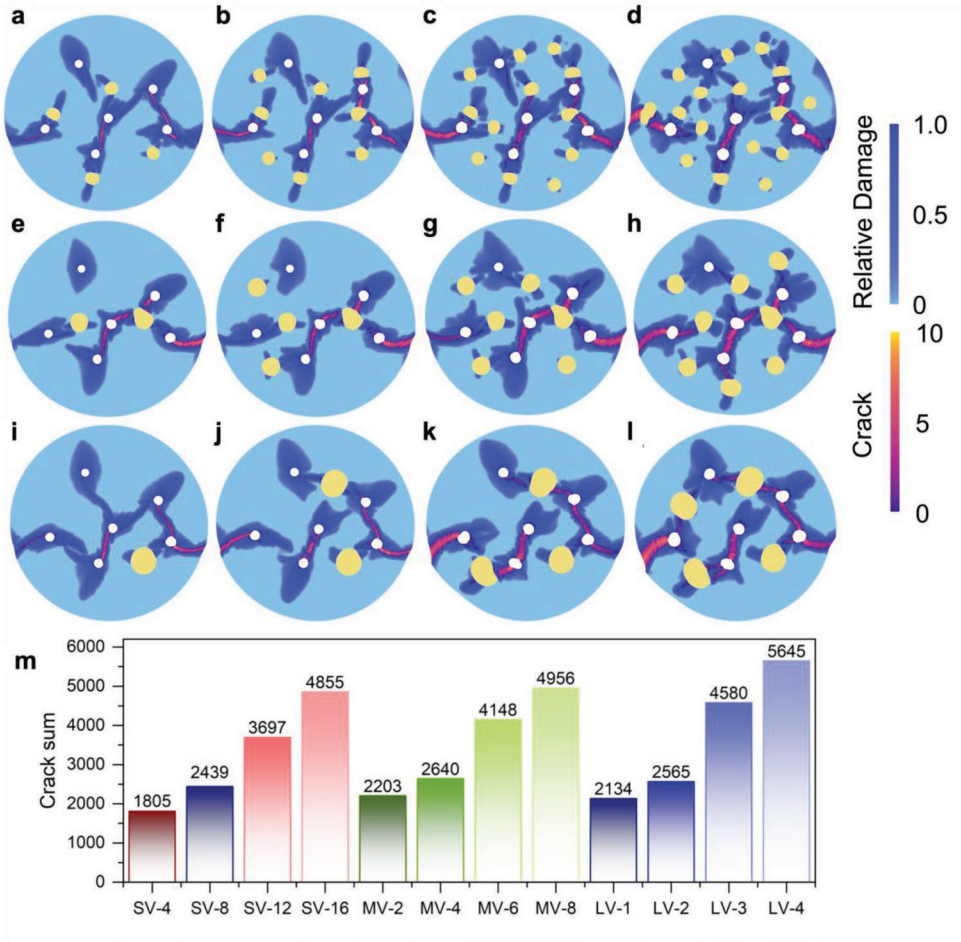

Figure 6. Effect of internal voids on mechanical failure of solid electrolyte. a–l) Relative damage and corresponding crack of solid electrolyte caused by growth of 6 Li filaments with presence of 4 (a), 8 (b), 12 (c), and 16 (d) small-size voids; 2 (e), 4 (f), 6 (g), and 8 (h) middle-size voids; and 1 (i), 2 (j), 3 (k), and 4 (l) large-size voids. Voids and Li filaments are corresponding to the brown regions and white regions, respectively. m) Total crack in solid electrolyte with voids and grown Li filaments.

the effect of the number of voids is greater than that of size on the failure behavior of solid electrolyte.

The abovementioned results indicate that the growth of Li filaments inside solid electrolyte leads to the locally high stress, displacement of material, and eventually mechanical failure of the pellet. This electro–chemo–mechanical process is strongly associated with the geometry, number, and size of Li filaments. Our results suggest that regulation of Li filaments growth inside solid electrolyte is as important as the design of solid electrolyte regarding to its electro–chemo–mechanical failure. Focusing more attention on the guiding of internal Li filament growth can be a new direction for the future design of solid electrolytes and solid-state cell configurations to suppress their electro–chemo–mechanical failure. Here are the strategies we proposed: 1) Suppressing Li nucleation in solid electrolyte. The internal Li filaments stem from the reduction and nucleation of Li in the solid electrolyte and suppressing the electron transfer process at Li filament/solid electrolyte interface can primarily prevent the electrochemical plating process. This can be explored by lowering the electronic conductivity of bulk solid electrolyte or introducing highly resistant interlayers between solid electrolyte and electrodes (cathode and anode). 2) Regulating the geometry of Li filaments inside solid electrolyte. Once the Li filaments are formed in solid electrolyte, the caused cracks highly prefer to propagate along the extended line of corner with great fluctuation. Therefore, improving physical contact between Li and solid electrolyte will reduce the fluctuation at interface, effectively suppressing the propagation of cracks. 3) Decrease the number density of Li filaments. Decreasing the presence of electrochemically unstable phase by tailoring the chemical design of solid electrolyte can ultimately suppress the formation of segregated Li and thus decrease the number density of Li filaments, which is more fatal to the failure of solid electrolyte.

Furthermore, our results also suggest that design of solid electrolyte from a perspective of fracture mechanics is of high significance to the mechanical degradation of solid electrolyte and unfortunately this is barely mentioned in previous reports, which mainly involve in the design of solid electrolyte at material level. For example, our work shows that the number density of pre-existing voids in the solid electrolyte pellet also plays a critical role on the crack propagation inside. Considering the

internal voids of same volume in total, the porosity formed by small voids will contribute to higher number density of voids and thus speed up the propagation of cracks in solid electrolyte. Therefore, advanced sintering techniques, like ultrafast high-temperature sintering[32] or well controlled grain size,[33,34] can be explored to decrease the porosity particularly that from small voids, for obtaining a low number density of voids as well as a mechanically robust solid electrolyte pellet for tolerating the internal electroplating of Li. Apart from this case, there are plenty of design strategies on suppressing the propagation of cracks in solid materials and it will be an distinctive direction for the field of solid-state batteries.

Last but not the least, it is worth noting that the LAGP solid electrolyte in our simulation work is treated as a continuum without regarding the material or chemistry, and its properties extracted from experimental data are introduced as input for the calculation process. In addition, related experimental results are absorbed for the fabrication of the model on each occasion. On one hand, this treatment for modeling promises the minimized difference between simulation conditions and the real situation in electrochemical systems. On the other hand, our model can be easily transferred into the simulation of other solid electrolyte systems, such as garnet, sulfide, or argyrodite, for understanding electro–chemo–mechanical failure of solid electrolyte as well as solid-state cells built with these electrolytes.

3. Conclusion

An electro–chemo–mechanical modeling for the failure process of solid electrolyte induced by the growth of internal Li filaments has been conducted in our work. The visualization of stress field, local displacement, and relative damage reveals the formation of cracks and their further propagation inside solid electrolyte, which results in the mechanical degradation and final disintegration of solid electrolyte pellet. We show that the local displacement of solid electrolytes is generated by the stress field, invariably leading to the damage of solid electrolyte inside and the formation of cracks. The anisotropic stress field as well as the separated displacement field, which are resulted from the geometry of a single Li filament, aggravates the damage of solid electrolyte. Moreover, the number and size of multiple Li filaments in the solid electrolyte pellet are crucial to the distribution of stress field and local displacement. It is found that the Li filaments with small diameter, but high number density promote the formation of integrated network for stress field between adjacent filaments, resulting in a fast propagation of damage in solid electrolyte. The size of pre-existing voids in a real solid electrolyte pellet, usually formed during sintering, shows less influence on the failure process compared to their number and thus reducing the porosity of solid electrolyte is a reliable way to suppress its degradation under the internal electroplating of Li. Our findings provide distinctive insights of Li filament growth and fracture mechanics into the design of future solid electrolytes for suppressing their mechanical failure caused by electroplating of Li inside, paving the way to the fabrication of high-performance solid-state Li-metal batteries. Furthermore, the knowledge and developed methodologies for growth of metal filaments in solid electrolytes are of high relevance also for other research in the area of solid state ionics, such as memristors.

4. Experimental Section

Electro–Chemo–Mechanical Model: In this study, the properties of NASICON-type electrolyte LAGP were used to simulate the bulk solid electrolyte, as listed in Table S2, Supporting Information. The electroplating of Li filament inside solid electrolyte could be sorted as the mass-transfer process of Li-ion and successive electron-transfer for reduction, which can be simplified as

$$Li^+ + e^- \rightleftharpoons Li \tag{1}$$

The relationship between overpotential and Faradic current density of the above electrochemical reaction can be described with the Butler–Volmer equation:[35,36]

$$i = i_0\left[\exp\left(\frac{\alpha F}{RT}\Phi\right) - \exp\left(-\frac{\beta F}{RT}\Phi\right)\right. \tag{2}$$

where i is the Faradic current density, i_0 is the exchange current density, F is the Faradic constant, R is the ideal gas constant, T is the Kelvin temperature, α and β are the charge-transfer coefficients for anodic and cathodic reactions ($\alpha + \beta = 1$), and Φ is the overpotential at the Li filament/solid electrolyte interface.

Based on Equation (2), the ongoing reduction of Li-ions to form Li atoms is driven by the overpotential at the Li filament/solid electrolyte interface, which is determined by the interfacial state and yielded as[37]

$$\Phi = \eta_s + \eta_m + \Delta\mu_{e^-} \tag{3}$$

where η_s is the surface overpotential, η_m is the overpotential caused by mass-transfer, and it is governed by the Fick's laws. $\Delta\mu_{e^-}$ is the overpotential caused by the deformation at steady-state motion.[38,39] Based on the theory created by Monroe and Newman,[39,40] $\Delta\mu_{e^-}$ can be given as

$$\begin{aligned}\Delta\mu_{e^-} = &-\frac{1}{2}\left(\overline{V}_{Li} + t_{-}\overline{V}_{Li^+}\right)\times\left\{-2\gamma\kappa + n\left[\tau_d^{Li} - \tau_d^{LAGP}\right]\right\}\\ &+\frac{1}{2}\left(\overline{V}_{Li} - t_{-}\overline{V}_{Li^+}\right)\left(\Delta p_{Li} + \Delta p_{LAGP}\right)\end{aligned} \tag{4}$$

where $\overline{V}_i$ is the related molar volume of Li, γ is the surface energy of Li, κ is the mean curvature, n is the unit vector pointing from the Li filament to the solid electrolyte, τ_d is the deformation stress, and p is pressure.

Here, the focus was on the electro–chemo–mechanical processes after the filling of primary cracks/voids inside solid electrolyte with Li filaments. It was assumed that the plastic Li filaments inside the cracks/voids of solid electrolyte had a close contact, and the surrounding brittle solid electrolyte was treated as an entirety with locally homogeneous properties. Therefore, the quasi-static equilibrium of a continuum containing plastic deformation of Li filaments and crack propagation was applied to describe the relationship between stress, strain, and displacement during the development of fractures in solid electrolyte, which can be given as[41,42]

$$\nabla\cdot\sigma + \overline{b} = 0 \tag{5}$$

$$\varepsilon = \frac{1}{2}\left\{\nabla u + (\nabla u)^T\right\} \tag{6}$$

$$\sigma = (1 - D_\varepsilon)c : \varepsilon \tag{7}$$

where σ and c are the Cauchy stress tensor and elastic modulus tensor, respectively, $\overline{b}$ is the body force vector, ε is the strain tensor, u is the displacement vector, and D_ε is the parameter for relative damage.

Especially, D_ε is a scalar and represents the percentage of mechanical damage ($0 < D_\varepsilon < 1$). Equations (5) and (6) are solved following[41]

$$\int \nabla \delta u : \sigma d\mathbb{Q} = \int \nabla u \cdot \overline{b} d\mathbb{Q} + \int \nabla u \cdot \overline{m} d\mathbb{R} \tag{8}$$

where $\mathbb{Q}$ is the integral domain for the total contact area between the Li filament and the solid electrolyte, $\overline{m}$ is the surface traction vector, and $\mathbb{R}$ is the integral domain for damage surface.

Based on the modified von Mises criterion, the damage mechanics could be yielded with the equivalent strain–stress relationship:[43]

$$\varepsilon_e = \frac{\kappa - 1}{2\kappa(1-2\upsilon)} \mathbb{I}_1' + \frac{1}{2}\sqrt{\left(\frac{\kappa-1}{1-2\upsilon}\mathbb{I}_1'\right)^2 + \frac{12\kappa}{(1+\upsilon)^2}\mathbb{J}_2'} \tag{9}$$

where ε_e is equivalent strain, κ is the ratio between tensile and compressive strength, υ is Poisson's ratio, $\mathbb{I}_1'$ is the first invariant of the strain tensor, and $\mathbb{J}_2'$ the second invariant of the deviatoric strain tensor.

Next, the competitive relationship between cohesive traction and crack-opening displacement on crack surface (τ) was used to describe the evolution of damage:[44]

$$\tau = \sigma_0 \exp\left(-\frac{\sigma_0}{G_f} u_C\right) \tag{10}$$

where σ_0 was the initial stress of fracture, G_f was fracture energy of solid electrolyte, and u_C was displacement of crack. Substituting $\tau = \sigma_e$ (equivalent stress based on Hooke's law), $\sigma_0 = E\varepsilon_0$, and $u_C = L(\varepsilon_e - \varepsilon_0)$ into Equation (10), the equivalent strain can be yielded as follows:

$$\sigma_e = \left[1 - \left(1 - \frac{\varepsilon_0}{\varepsilon_e}\exp\left(-\frac{E\varepsilon_0 L}{u_C}(\varepsilon_e - \varepsilon_0)\right)\right)\right] E\varepsilon_e \tag{11}$$

where E is the Young's modulus of thsolid electrolyte and L the length of evolving damage in unit. Therefore, the damage function could be obtained after comparing Equations (7) and (11) as

$$D(\varepsilon_e) = 1 - \frac{\varepsilon_0}{\varepsilon_e}\exp\left(-\frac{E\varepsilon_0 L}{u_C}(\varepsilon_e - \varepsilon_0)\right) \tag{12}$$

Multiphysics Simulations: All the simulations in this work, including model construction, solution, data analysis, and processing, were conducted by using the electrochemical module and solid mechanics module in COMSOL Multiphysics software channeled with MATLAB and Python script. The parameters for the electro–chemo–mechanical modeling are listed in Table S1, Supporting Information. Extremely fine mesh division of the model with a maximum mesh size of 0.05 μm was employed to maximize the accuracy of simulation. As mentioned previously, the solid electrolyte and Li filaments were treated as homogeneous and isotropic solid materials in the model. A numerical damage model was used to describe the damage process of solid electrolyte. To build the model with multiple Li filaments or voids, a random distribution of coordinates in the fixed area was conducted in MATLAB.

The initial state of the model assumed that the Li filaments had just filled the cracks/voids in the solid electrolyte without generation of stress at Li/solid electrolyte interface. Under the electrochemical condition, the growth of Li filaments was simulated based on the mass transfer process of Li-ion in solid electrolyte and the deposition process of metallic Li at the interface with solid electrolyte, triggering the expansion of Li filaments. Therefore, local stress was applied to the outer wall of the solid electrolyte, leading to elastic compression, damage of solid electrolyte, and cracks propagation, until thorough disintegration of solid electrolyte. The relative tolerance of the solution process was 0.0001, and the limit solution time was 50 units of calculation time.

Supporting Information

Supporting Information is available from the Wiley Online Library or from the author.

Acknowledgements

This work is supported by Batteries Sweden (BASE), Chalmers Areas of Advance Materials Science and Energy. The authors thank the National Natural Science Foundation of China (U21B2057 and 51802256), and China Scholarship Council (No. 201908090043) for supporting this work.

Conflict of Interest

The authors declare no conflict of interest.

Data Availability Statement

The data that support the findings of this study are available from the corresponding author upon reasonable request.

Keywords

electro–chemo–mechanics, lithium filaments, mechanical failures, solid electrolytes, solid-state batteries

Received: August 9, 2022
Revised: September 9, 2022
Published online:

[1] C. P. Grey, D. S. Hall, *Nat. Commun.* **2020**, *11*, 6279.
[2] H. Au, M. Crespo-Ribadeneyra, M.-M. Titirici, *One Earth* **2022**, *5*, 207.
[3] M. Balaish, J. C. Gonzalez-Rosillo, K. J. Kim, Y. Zhu, Z. D. Hood, J. L. M. Rupp, *Nat. Energy* **2021**, *6*, 227.
[4] P. G. Bruce, S. A. Freunberger, L. J. Hardwick, J. M. Tarascon, *Nat. Mater.* **2011**, *11*, 19.
[5] J. M. Tarascon, M. Armand, *Nature* **2001**, *414*, 359.
[6] C. C. Fang, J. X. Li, M. H. Zhang, Y. H. Zhang, F. Yang, J. Z. Lee, M. H. Lee, J. Alvarado, M. A. Schroeder, Y. Y. C. Yang, B. Y. Lu, N. Williams, M. Ceja, L. Yang, M. Cai, J. Gu, K. Xu, X. F. Wang, Y. S. Meng, *Nature* **2019**, *572*, 511.
[7] Y. Liu, X. Xu, O. O. Kapitanova, P. V. Evdokimov, Z. Song, A. Matic, S. Xiong, *Adv. Energy Mater.* **2022**, *12*, 2103589.
[8] X. Xu, X. Jiao, O. O. Kapitanova, J. Wang, V. S. Volkov, Y. Liu, S. Xiong, *Adv. Energy Mater.* **2022**, *12*, 2200244.
[9] A. Manthiram, X. Yu, S. Wang, *Nat. Rev. Mater.* **2017**, *2*, 16103.
[10] S. Sarkar, V. Thangadurai, *ACS Energy Lett.* **2022**, *7*, 1492.
[11] J. Kasemchainan, S. Zekoll, D. S. Jolly, Z. Ning, G. O. Hartley, J. Marrow, P. G. Bruce, *Nat. Mater.* **2019**, *18*, 1105.
[12] Y. Lu, C.-Z. Zhao, H. Yuan, X.-B. Cheng, J.-Q. Huang, Q. Zhang, *Adv. Funct. Mater.* **2021**, *31*, 2009925.
[13] F. Han, A. S. Westover, J. Yue, X. Fan, F. Wang, M. Chi, D. N. Leonard, N. J. Dudney, H. Wang, C. Wang, *Nat. Energy* **2019**, *4*, 187.
[14] L. Porz, T. Swamy, B. W. Sheldon, D. Rettenwander, T. Frömling, H. L. Thaman, S. Berendts, R. Uecker, W. C. Carter, Y.-M. Chiang, *Adv. Energy Mater.* **2017**, *7*, 1701003.
[15] Z. Ning, D. S. Jolly, G. Li, R. De Meyere, S. D. Pu, Y. Chen, J. Kasemchainan, J. Ihli, C. Gong, B. Liu, D. L. R. Melvin, A. Bonnin, O. Magdysyuk, P. Adamson, G. O. Hartley, C. W. Monroe, T. J. Marrow, P. G. Bruce, *Nat. Mater.* **2021**, *20*, 1121.
[16] J. Tippens, J. C. Miers, A. Afshar, J. A. Lewis, F. J. Q. Cortes, H. Qiao, T. S. Marchese, C. V. Di Leo, C. Saldana, M. T. McDowell, *ACS Energy Lett.* **2019**, *4*, 1475.

[17] J. A. Lewis, F. J. Q. Cortes, Y. Liu, J. C. Miers, A. Verma, B. S. Vishnugopi, J. Tippens, D. Prakash, T. S. Marchese, S. Y. Han, C. Lee, P. P. Shetty, H. W. Lee, P. Shevchenko, F. De Carlo, C. Saldana, P. P. Mukherjee, M. T. McDowell, *Nat. Mater.* **2021**, *20*, 503.
[18] X. Liu, R. Garcia-Mendez, A. R. Lupini, Y. Cheng, Z. D. Hood, F. Han, A. Sharafi, J. C. Idrobo, N. J. Dudney, C. Wang, C. Ma, J. Sakamoto, M. Chi, *Nat. Mater.* **2021**, *20*, 1485.
[19] S. Hao, S. R. Daemi, T. M. M. Heenan, W. Du, C. Tan, M. Storm, C. Rau, D. J. L. Brett, P. R. Shearing, *Nano Energy* **2021**, *82*, 105744.
[20] E. Kazyak, R. Garcia-Mendez, W. S. LePage, A. Sharafi, A. L. Davis, A. J. Sanchez, K.-H. Chen, C. Haslam, J. Sakamoto, N. P. Dasgupta, *Matter* **2020**, *2*, 1025.
[21] C. Yuan, W. Lu, J. Xu, *Adv. Energy Mater.* **2021**, *11*, 2101807.
[22] F. Liu, R. Xu, Y. Wu, D. T. Boyle, A. Yang, J. Xu, Y. Zhu, Y. Ye, Z. Yu, Z. Zhang, X. Xiao, W. Huang, H. Wang, H. Chen, Y. Cui, *Nature* **2021**, *600*, 659.
[23] R. S. Gordon, G. R. Miller, B. J. McEntire, E. D. Beck, J. R. Rasmussen, *Solid State Ionics* **1981**, *3-4*, 243.
[24] W. Liu, X. Sun, M. A. Khaleel, *J. Power Sources* **2008**, *185*, 1193.
[25] L. Yang, X. Huang, C. Zou, X. Tao, L. Liu, K. Luo, P. Zeng, Q. Dai, Y. Li, L. Yi, Z. Luo, X. Wang, *Ceram. Int.* **2021**, *47*, 18196.
[26] T. Krauskopf, R. Dippel, H. Hartmann, K. Peppler, B. Mogwitz, F. H. Richter, W. G. Zeier, J. Janek, *Joule* **2019**, *3*, 2030.
[27] H. Lim, S. Jun, Y. B. Song, H. Bae, J. H. Kim, Y. S. Jung, *Energy Storage Mater.* **2022**, *50*, 543.
[28] Y. Pang, J. Pan, J. Yang, S. Zheng, C. Wang, *Electrochem. Energy Rev.* **2021**, *4*, 169.
[29] J. Wu, L. Shen, Z. Zhang, G. Liu, Z. Wang, D. Zhou, H. Wan, X. Xu, X. Yao, *Electrochem. Energy Rev.* **2021**, *4*, 101.
[30] B. J. Mcentire, R. A. Bartlett, G. R. Miller, R. S. Gordon, *J. Am. Ceram. Soc.* **1983**, *66*, 738.
[31] S.-H. Leigh, C. C. Berndt, *J. Am. Ceram. Soc.* **1999**, *82*, 17.
[32] C. Wang, W. Ping, Q. Bai, H. Cui, R. Hensleigh, R. Wang, A. H. Brozena, Z. Xu, J. Dai, Y. Pei, *Science* **2020**, *368*, 521.
[33] J. Svoboda, H. Riedel, *Acta Metall. Mater.* **1992**, *40*, 2829.
[34] R. W. Rice, S. W. Freiman, P. F. Becher, *J. Am. Ceram. Soc.* **1981**, *64*, 345.
[35] E. J. F. Dickinson, A. J. Wain, *J. Electroanal. Chem.* **2020**, *872*, 114145.
[36] S. D. Fabre, D. Guy-Bouyssou, P. Bouillon, F. L. Cras, C. Delacourt, *J. Electrochem. Soc.* **2011**, *159*, A104.
[37] S.-L. Wu, A. E. Javier, D. Devaux, N. P. Balsara, V. Srinivasan, *J. Electrochem. Soc.* **2014**, *161*, A1836.
[38] P. Barai, K. Higa, V. Srinivasan, *Phys. Chem. Chem. Phys.* **2017**, *19*, 20493.
[39] C. Monroe, J. Newman, *J. Electrochem. Soc.* **2005**, *152*, A396.
[40] C. Monroe, J. Newman, *J. Electrochem. Soc.* **2004**, *151*, A880.
[41] M. Kurumatani, Y. Soma, K. Terada, *Eng. Fract. Mech.* **2019**, *206*, 392.
[42] M. Kurumatani, K. Terada, J. Kato, T. Kyoya, K. Kashiyama, *Eng. Fract. Mech.* **2016**, *155*, 49.
[43] J. H. P. de Vree, W. A. M. Brekelmans, M. A. J. van Gils, *Comput. Struct.* **1995**, *55*, 581.
[44] G. N. Wells, L. J. Sluys, *Eng. Fract. Mech.* **2000**, *65*, 263.